

Land-sea coupling of early Pleistocene glacial cycles in the southern North Sea exhibit dominant Northern Hemisphere forcing

Timme H. Donders^{1,2}, Niels A.G.M. van Helmond³, Roel Verreussel², Dirk Munsterman⁴, Johan Ten Veen⁴, Robert P. Speijer⁵, Johan W.H. Weijers^{3*}, Francesca Sangiorgi³, Francien Peterse³, Gert-Jan Reichert^{3,6}, Jaap S. Sinninghe Damsté^{3,6}, Lucas Lourens³, Gesa Kuhlmann⁷ and Henk Brinkhuis^{3,6}

¹ Department of Physical Geography, Fac. of Geosciences, Utrecht University, Heidelberglaan 2, 3584CD, Utrecht, The Netherlands.

² TNO - Applied Geosciences, Netherlands Organisation of Applied Scientific Research Princetonlaan 6, 3584 CB Utrecht, The Netherlands.

³ Department of Earth Sciences, Fac. of Geosciences, Utrecht University, Heidelberglaan 2, 3584CS, Utrecht, The Netherlands.

⁴ TNO - Geological Survey of the Netherlands, Netherlands Organisation of Applied Scientific Research, Princetonlaan 6, 3584 CB Utrecht, The Netherlands.

⁵ Department of Earth and Environmental Sciences, KU Leuven, 3001 Heverlee, Belgium

⁶ NIOZ Royal Netherlands Institute for Sea Research, P.O. Box 59, 1790 AB, Den Burg, Texel, The Netherlands

⁷ BGR - Federal Institute for Geosciences and Natural Resources, Geozentrum Hannover Stilleweg 2, D-30655 Hannover

* Currently at: Shell Global Solutions International B.V., Grasweg 31, 1031 HW, Amsterdam, The Netherlands

Correspondence to: t.h.donders@uu.nl

Abstract

We assess the disputed phase relations between forcing and climatic response in the early Pleistocene with a spliced Gelasian (~2.6 – 1.8 Ma) multi-proxy record from the southern North Sea basin. The cored sections couple climate evolution on both land and sea during the intensification of Northern Hemisphere Glaciations (NHG) in NW Europe, providing the first well-constrained stratigraphic sequence of the classic terrestrial Praetiglian Stage. Terrestrial signals were derived from the Eridanos paleoriver, a major fluvial system that contributed a large amount of freshwater to the northeast Atlantic. Due to its latitudinal position, the Eridanos catchment was likely affected by early Pleistocene NHG, leading to intermittent shutdown and reactivation of river flow and sediment transport. Here we apply organic geochemistry, palynology, carbonate isotope geochemistry, and seismostratigraphy to document both vegetation changes in the Eridanos catchment and regional surface water conditions and relate them to early Pleistocene glacial-interglacial cycles and relative sea-level changes. Paleomagnetic and palynological data provide a solid integrated timeframe that ties the obliquity cycles, expressed in the borehole geophysical logs, to Marine Isotope Stages (MIS) 103 to 92, independently confirmed by a local benthic oxygen isotope record. Marine and terrestrial palynological and organic geochemical records provide high resolution reconstructions of relative Terrestrial and Sea Surface Temperature (TT and SST), vegetation, relative sea level, and coastal influence.

During the prominent cold stages MIS 98 and 96, as well as MIS 94 the record indicates increased non-arboreal vegetation, and low SST and TT, and low relative sea level. During the warm stages MIS 99, 97 and 95 we infer increased stratification of the water column together with higher % arboreal vegetation, high SST and relative sea-level maxima. The early Pleistocene distinct warm-cold alterations are synchronous between land and sea, but lead the relative sea-level change by 3-8 thousand years. The record provides evidence for a

51 dominantly NH driven cooling that leads the glacial build up and varies on obliquity
52 timescale. Southward migration of Arctic surface water masses during glacials, indicated by
53 cool-water dinoflagellate cyst assemblages, is furthermore relevant for the discussion on the
54 relation between the intensity of the Atlantic meridional overturning circulation and ice sheet
55 growth.

56

57 **Keywords:** Glacial-interglacial climate, palynology; organic geochemistry; obliquity, land-
58 sea correlation, Eridanos delta, southern North Sea

1 Introduction

The build-up of extensive Northern Hemisphere (NH) land ice started around 3.6 Ma ago (Ruddiman et al. 1986; Mudelsee and Raymo, 2005; Ravelo et al., 2004; Ravelo, 2010), with stepwise intensifications between 2.7 and 2.54 Ma ago (e.g., Shackleton and Hall, 1984; Raymo et al., 1989; Haug et al., 2005; Lisiecki and Raymo, 2005; Sosdian and Rosenthal, 2009). In the North Atlantic region the first large-scale early Pleistocene glaciations, Marine Isotope Stages (MISs) 100 - 96, are marked by e.g. appearance of ice-rafted debris and southward shift of the Arctic front (see overviews in Naafs et al., 2013; Hennissen et al., 2015). On land, the glaciations led to faunal turnover (e.g. Lister, 2004; Meloro et al., 2008) and widespread vegetation changes (e.g. Zagwijn, 1992; Hooghiemstra and Ran, 1994; Svenning, 2003; Brigham-Grette et al., 2013). Many hypotheses have been put forward to explain the initiation of these NH glaciations around the Plio-Pleistocene transition interval. Causes include tectonics (Keigwin, 1982, Raymo, 1994; Haug and Tiedemann, 1998; Knies et al., 2004; Poore et al., 2006), orbital forcing dominated by obliquity-paced variability (Hays et al., 1976; Maslin et al., 1998; Raymo et al., 2006) and atmospheric CO₂ concentration decline (Pagani et al., 2010; Seki et al., 2010; Bartoli et al., 2011) driven by e.g. changes in ocean stratification that affected the biological pump (Haug et al., 1999). Changes were amplified by NH albedo changes (Lawrence et al., 2010), evaporation feedbacks (Haug et al., 2005), and possibly tropical atmospheric circulation change and breakdown of a permanent El Niño (Ravelo et al., 2004; Brierley and Fedorov, 2010; Etourneau et al., 2010).

Key aspects in this discussion are the phase relations between temperature change on land, in the surface and deep ocean, and ice sheet accretion (expressed through global eustatic sea-level lowering) in both Northern and Southern Hemispheres. According to Raymo et al.

(2006), early Pleistocene obliquity forcing dominated global sea level and $\delta^{18}\text{O}_{\text{benthic}}$, because precession-paced changes in the Greenland and Antarctic ice sheets cancelled each other out. In this view, climate records independent of sea-level variations should display significant variations on precession timescale. Recent tests of this hypothesis indicate that early Pleistocene precession signals are prominent in both Laurentide ice sheet meltwater pulses and iceberg-rafted debris of the East Antarctic ice sheet, and decoupled from marine $\delta^{18}\text{O}$ (Patterson et al., 2014; Shakun et al., 2016). Alternatively, variations in the total integrated summer energy, which is obliquity controlled, might be responsible for the dominant obliquity pacing of the early Pleistocene (Huybers, 2011; Tzedakis et al., 2017). The dominance of the obliquity component has been attributed to feedbacks between high-latitude insolation, albedo (sea-ice and vegetation) and ocean heat flux (Koenig et al., 2011; Tabor et al., 2014). Sosdian and Rosenthal (2009) suggested that temperature variations, based on benthic foraminifer magnesium/calcium (Mg/Ca) ratios from the North Atlantic, explain a substantial portion of the global variation in the $\delta^{18}\text{O}_{\text{benthic}}$ signal. Early Pleistocene North Atlantic climate responses were closely phased with $\delta^{18}\text{O}_{\text{benthic}}$ changes, evidenced by dominant 41-kyr variability in North American biomarker dust fluxes at IODP Site U1313 (Naafs et al., 2012), suggesting a strong common NH high latitude imprint on North Atlantic climate signals (Lawrence et al., 2010). Following this reasoning, glacial build-up should be in phase with decreases in NH sea surface temperatures (SST) and terrestrial temperatures (TT).

To explicitly test this hypothesis we perform a high-resolution multiproxy terrestrial and marine palynological, organic geochemical, and stable isotope study on a marginal marine sediment sequence from the southern North Sea (SNS) during the early Pleistocene “41 kyr-world”. We investigate the leads and lags of regional marine vs. terrestrial climatic cooling

during MIS 102-92, and assess the local sea-level response relative to global patterns from the $\delta^{18}\text{O}_{\text{benthic}}$ stack of Lisiecki and Raymo (2005; LR04). In a dominantly, NH obliquity driven scenario, we expect the marine and terrestrial temperature proxies to be in phase on obliquity timescales with a short (less than 10 kyr) lead on sea-level variations. In addition, the record can better constrain the signature and timing of the regional continental Praetigian stage (Van der Vlerk and Florschütz, 1953; Zagwijn, 1960) that is still widely used, although its stratigraphic position and original description are not well defined (Donders et al., 2007; Kemna and Westerhoff, 2007).

2 Geological setting

During the Neogene the epicontinental North Sea Basin was confined by landmasses except towards the northwest, where it opened into the Atlantic domain (Fig. 1) (Bijlsma, 1981; Ziegler, 1990). Water depths in the central part were approximately between 100 to 300 m as deduced from seismic geometry (Huuse et al., 2001; Overeem et al., 2001). In contrast, the recent North Sea has an average depth between 20-50 m in the south that deepens only towards the shelf edge towards 200 m in the north-west (e.g., Caston, 1979). From the present-day Baltic region a formidable river system, known as the Eridanos paleoriver, developed which built up the Southern North Sea delta across southern Scandinavia (Sørensen et al., 1997; Michelsen et al., 1998; Huuse et al., 2001; Overeem et al., 2001).

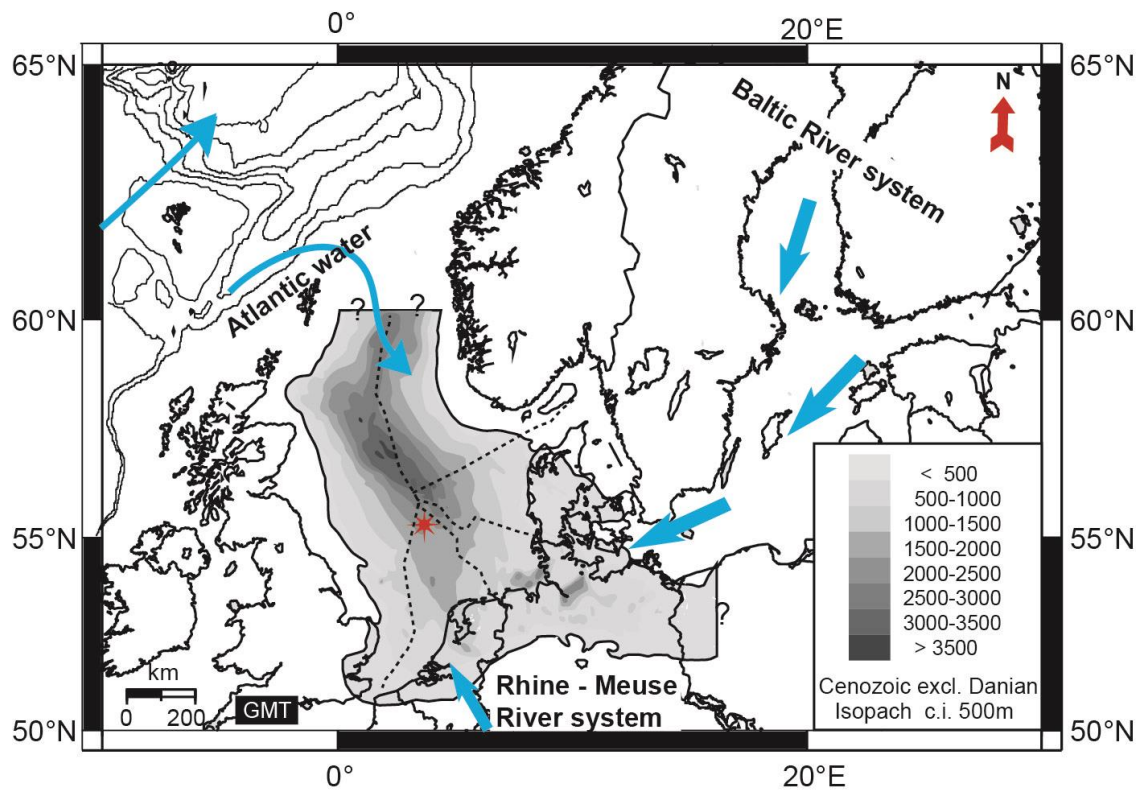


Figure 1: Geographical map of the present day North Sea region with the superimposed thickness of Cenozoic sediment infill after Ziegler (1990) and the offshore sectors (dashed lines). The reconstructed different water sources (see Gibbard and Lewin, 2016) that influenced the Pliocene and early Pleistocene North Sea hydrography, including the freshwater supply of the Baltic river system, the Rhine-Meuse river system and Atlantic surface waters are indicated with blue arrows. The location of both boreholes A15-3 (UTM X 552567.1, Y 6128751.6) and A15-4 (UTM X 557894.4, Y 6117753.5) is marked by an asterisk, see Fig. S1 for details.

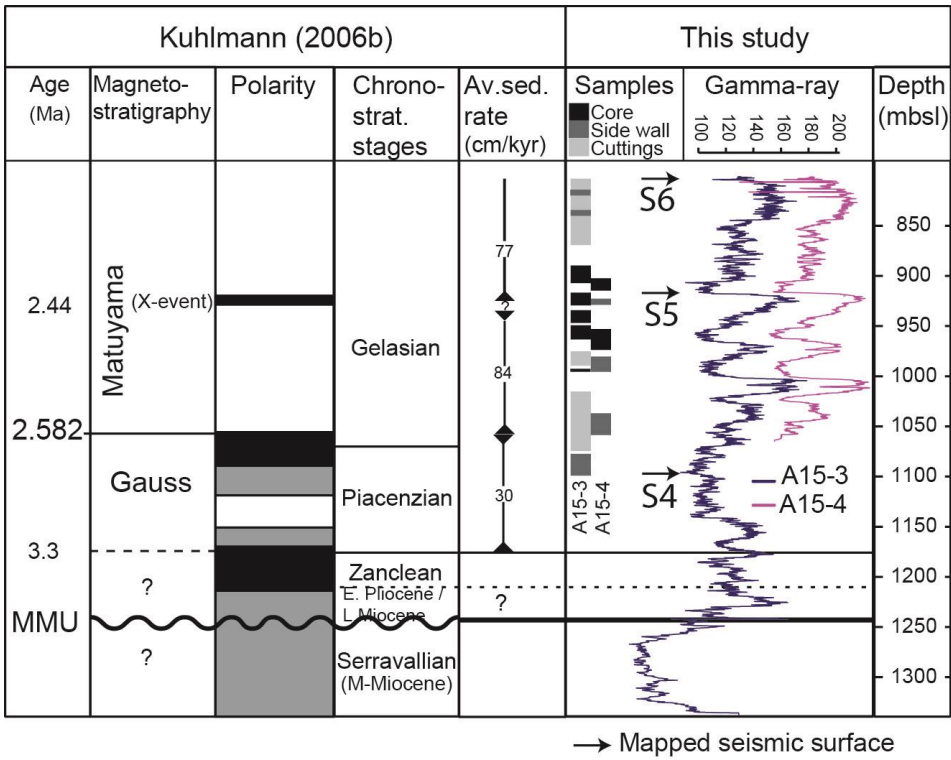
This delta was characterized by an extensive distributary system that supplied large amounts of freshwater and sediment to the shelf sea during the Neogene and early Pleistocene (Overeem et al., 2001), resulting in a sediment infill of ~1500 m in the central North Sea Basin (Fig. 1). This system was fed by rainfall as well as by melt-water originating from Scandinavian glaciers (Kuhlmann et al., 2004), principally from the Baltic Shield in the east

with some contribution from the south (Fig. 1) (Bijlsma, 1981; Kuhlmann, 2004). The sedimentation rates reached up to 84 cm/kyr at the studied locations (Fig. 2) (Kuhlmann et al., 2006b). Today, the continental river runoff contributes only 0.5 % of the water budget in the North Sea (Zöllmer and Irion, 1996) resulting in sedimentation rates ranging between 0.4 to 1.9 cm/kyr in the Norwegian Channel, and 0.5 - 1 cm/kyr in the southern part of the North Sea (de Haas et al., 1997).

3 Material, core description and age model

Recent exploration efforts in the SNS led to the successful recovery of cored sedimentary successions of marine isotope stages (MIS) 102-92 and continuous paleomagnetic logs (Fig. 2) (Kuhlman et al, 2006ab). For quantitative palynological and geochemical analyses, discrete sediment samples were taken from two exploration wells A15-3 and A15-4 located in the northernmost part of the Dutch offshore sector in the SNS at the Neogene sedimentary depocentre (Fig. 1). An integrated age model is available based on a multidisciplinary geochronological analysis of several boreholes within the SNS (Kuhlmann et al., 2006a,b) and dinocyst biostratigraphy. The magnetostratigraphy, core correlation and age-diagnostic dinocyst events used for this age-model are summarized in Fig. 2 and Table S1. The recovered material mainly consists of fine-grained, soft sediments (clayey to very fine sandy), sampled from cuttings, undisturbed sidewall cores and core sections (Fig. 2). Geochemical analyses were limited to the (sidewall) core intervals, while the cuttings were to increase resolution of the palynological samples, and are based on larger rock chips that have been cleaned before treatment. Clear cyclic variations in the gamma ray signal and associated seismic reflectors across the interval can be correlated across the entire basin (Kuhlman et al., 2006a; Kuhlmann and Wong, 2008; Thöle et al. 2014). Samples from the two boreholes were spliced based on the gamma-ray logs (Figs. 2, S2) and biostratigraphic events to generate a

composite record. The age model is mainly based on continuous paleomagnetic logging supported by discrete sample measurements and high-resolution biostratigraphy. There is evidence of small hiatuses above (~2.1 Ma) and significant hiatuses below the selected interval (within the early Pliocene and Miocene, particularly the Mid-Miocene Unconformity), which is why we excluded these intervals in this study. The position of the Gauss-Matuyama transition at the base of log unit 6 correlates to the base of MIS 103, the identification of the X-event, at the top of log unit 9, correlates to MIS 96, and the Olduvai magnetochron is present within log units 16-18 (Kuhlmann et al., 2006a,b). These ages are supported by dinocyst and several other bioevents (Table S1, updated from Kuhlmann et al., 2006a,b). Consistent with the position of the X-event, the depositional model by Kuhlmann and Wong (2008) relates the relatively coarse-grained, low gamma ray intervals to interglacials characterized by high run off. A recent independent study on high-resolution stable isotope analyses of benthic foraminifera from an onshore section in the same basin confirmed this phase relation (Noorbergen et al., 2015). Around glacial terminations, when sea level was lower but the basin remained fully marine, massive amounts of very fine-grained clayey to fine silty material were deposited in the basin, the waste-products of intense glacial erosion. During interglacials with high sea level more mixed, coarser-grained sediments characterize the deposits, also reflecting a dramatically changed hinterland, retreated glaciers, and possibly (stronger) bottom currents (Kuhlmann and Wong, 2008). Based on this phase relation, detailed magneto- and biostratigraphy, grain size measurements, and previous low resolution relative SST indices (Kuhlmann et al., 2004; Kuhlmann et al., 2006a,b), the finer grained units are consistently correlated to MIS 102 – 92. Based on this correlation of the GR inflection points to the corresponding LR04 MIS transitions, the sequence is here transferred to an age scale through interpolation with a smoothing spline function (Fig. S3).



192

193

194

195

196

197

198

199

200

201

202

203

204

205

206

Figure 2: Chronology and mean sedimentation rates as derived from biostratigraphy and paleomagnetic data (Kuhlmann et al., 2006a,b) in combination with the gamma-ray log of A15-3 and A15-4 used in this study on a common depth scale. The position of various sample types and the mapped seismic horizons S4-6 (Fig. S1) are indicated. Material for the sidewall cores is limited, and used only for palynology and organic geochemistry. Bioevents based on Kuhlmann et al. (2006a,b) are listed in Table S1.

The regional structure and development of the delta front across the Plio-Pleistocene transition interval is very well constrained by a high-resolution regional geological model that represents the anatomy of the Eridanos (pro-) delta (Kuhlmann and Wong, 2008; Ten Veen et al., 2013). A total of 25 seismic horizons in the Plio-Pleistocene transition interval were mapped using series of publically available 2D and 3D seismic surveys across the northern part of the Dutch offshore sector. For all these surfaces the distribution of delta elements such as of topset-, foreset- and toeset-to-prodelta has been determined, resulting in zonal maps

(250 m grid size) that represent the present day geometry of the surfaces. The paleoenvironmental reconstructions are compared to these maps to constrain the regional setting and aid the interpretations.

4 Paleoenvironmental proxies and methods

4.1 Benthic oxygen and carbon isotopes ($\delta^{18}O_b$ and $\delta^{13}C_b$)

Oxygen and carbon isotopes were measured on tests of *Cassidulina teretis*, a cold water species of endobenthic foraminifera that is generally abundant in the samples and common in fine-grained sediment and relatively low salinities (Mackensen and Hald, 1988; Rosoff and Corliss, 1992). Because of their endobenthic habitat, they record isotope compositions of pore waters, which leads to somewhat reduced ($\delta^{13}C_b$) values compared to the overlying bottom waters. Since the amount of material from the sidewall cores is limited, the isotope data is only produced for the cored intervals with the principal aim to confirm the phase relationship described by Kuhlmann and Wong (2008) between facies and climate. Preservation was based on a visual inspection and assignment of a relative preservation scale of 1-5, after which the poorest 2 classes were discarded because primary calcite was nearly absent. The best preserved specimens (cat. 1) had shiny tests (original wall calcite) and showed no signs of overgrowth. Category 2 specimens showed signs of overgrowth but were not recrystallized and cat. 3 specimens were dull and overgrown by a thin layer of secondary calcite. Between ~20 and 50 μg of specimens per sample was weighed after which the isotopes of the carbonate were measured using a Kiel III device coupled to a 253 ThermoFinnigan MAT instrument. Isotope measurements were normalized to an external standard ‘NBS-19’ ($\delta^{18}\text{O} = -2.20\text{‰}$, $\delta^{13}\text{C} = 1.95\text{‰}$).

4.2 Palynological proxies

In modern oceans, dinoflagellates are an important component of the (phyto-)plankton. About 15-20% of the marine dinoflagellates form an organic walled cyst (dinocyst) during the life cycle that can be preserved in sediments (Head, 1996). Dinocyst distribution in marine surface sediments has shown to reflect changes in the sea surface water properties, mostly responding to temperature (e.g., Rochon et al., 1999; Zonneveld et al., 2013). Down-core changes in dinocyst assemblages are widely used in reconstructing past environmental changes in the Quaternary (e.g., de Vernal et al., 2009), but also in the Neogene and Paleogene (e.g., Versteegh and Zonneveld, 1994; Head et al., 2004; Pross and Brinkhuis, 2005; Sluijs et al., 2005; Schreck et al., 2013; De Schepper et al., 2011; 2013; Hennissen et al., 2017).

Here we use the preference of certain taxa to cold-temperate to arctic surface waters to derive sea surface temperature (SST) trends. The cumulative percentage of the dinocysts *Filisphaera microornata*, *Filisphaera filifera*, *Filisphaera sp.*, *Habibacysta tectata* and *B. tepikiense* on the total dinocysts represents our cold surface water indicator (Versteegh and Zonneveld, 1994; Donders et al., 2009; De Schepper et al., 2011). Interestingly, *Bitectatodinium tepikiense*, the only extant dinocyst among our cold-water species, has been recorded from the mixing zone of polar front oceanic waters with cold brackish meltwaters from glacier ice (e.g., Bakken and Dale, 1986) and at the transition between the subpolar and temperate zones (Dale, 1996). The combined abundance of *Lingulodinium machaerophorum*, *Tuberculodinium vancampoe*, *Polysphaeridium zoharyi* and *Operculodinium israelianum* is used here to indicate, coastal waters, although they generally also relate to warmer conditions. In particular, high percentages of *L. machaerophorum* are typically recorded in eutrophic coastal areas where reduced salinity and (seasonal) stratification due to runoff occur (Dale, 1996; Sangiorgi and Donders, 2004; Zonneveld et al., 2009). At present, *T. vancampoe*, *P.*

zoharyi and *O. israelianum* are also found in lagoonal euryhaline environments (Zonneveld et al., 2013), and hence could be used to indicate a more proximal condition relative to *L. machaerophorum* (Pross and Brinkhuis, 2005).

At present, Protoperidinioid (P) cysts are mostly formed by heterotrophic dinoflagellates and the percentage of P-cysts may be used as indicator of high eukaryotic productivity (cf. Reichart and Brinkhuis, 2003; Sangiorgi and Donders, 2004; Sluijs et al., 2005). Here we use the percentage of P-cysts (*Brigantedinium* spp., *Lejeunecysta* spp., *Trinovantedinium glorianum*, *Selenopemphix* spp., *Islandinium* spp., *Barssidinium graminosum*, and *B. wrennii*) to indicate eukaryotic productivity.

Terrestrial palynomorphs (sporomorphs) reflect variations in the vegetation on the surrounding land masses and provide information on climate variables such as continental temperatures and precipitation (e.g. Heusser and Shackleton, 1979; Donders et al., 2009; Kotthoff et al., 2014). A ratio of terrestrial to marine palynomorphs (T/M ratio) is widely used as a relative measure of distance to the coast and thereby reflects sea-level variations and depth trends in the basin (e.g. McCarthy and Mudie, 1998; Donders et al., 2009; Quaijtaal et al., 2014; Kotthoff et al., 2014). Morphological characteristics of late Neogene pollen types can, in most cases, be related to extant genera and families (Donders et al., 2009; Larsson et al., 2011; Kotthoff et al., 2014). In A15-3/4, the relatively long distance between the land and the site of deposition means that the pollen assemblage is not only a reflection of vegetation cover and climate, but includes information on the mode of transport. Assemblages with a relatively high number of taxa, including insect pollinated forms, are indicative of substantial pollen input through water transport (Whitehead, 1983), whereas wind-transported pollen typically show a low-diversity. Sediments of a location proximal to a river delta likely receive

a majority of pollen that is water-transported, while distal locations are dominated by wind-transported pollen and particularly bisaccate taxa (Hooghiemstra, 1988; Mudie and McCarthy, 1994). To exclude these effects, the percentage of arboreal pollen (AP), representing relative terrestrial temperatures, was calculated excluding bisaccate forms. The non-arboreal pollen (NAP; mainly Poaceae and also *Artemisia*, Chenopodiaceae and Asteraceae) consist only of non-aquatic herbs. High AP percentages indicate warm, moist conditions, whereas open vegetation (NAP and Ericaceae) is indicative for cooler, drier conditions consistent with a glacial climate (Faegri et al, 1989).

4.3 Palynological processing

The samples were processed using standard palynological procedures (e.g., Faegri et al., 1989) involving HCl (30%) and cold HF (40%) digestion of carbonates and silicates. Residues were sieved with 15 µm mesh and treated by heavy liquid separation (ZnCl₂, specific gravity 2.1 g/cm³). The slides were counted for dinocysts (with a minimum of 100 cysts) and pollen (with a preferable minimum of 200 grains). The dinocyst taxonomy follows Williams et al. (2017). Resulting counts were expressed as percent abundance of the respective terrestrial or marine groups of palynomorphs.

4.4 Organic geochemical proxies

We applied three measures for the relative marine versus terrestrial hydrocarbon sources. The Carbon Preference Index (CPI), based on C₂₅-C₃₄ *n*-alkanes, originally devised to infer thermal maturity (Bray and Evans, 1961), has high values for predominantly terrestrial plant sources (Eglinton and Hamilton, 1967; Rieley et al., 1991). Values closer to one indicate greater input from marine microorganisms and/or recycled organic matter (e.g., Kennicutt et al., 1987). Furthermore, peat mosses like *Sphagnum* are characterized by a dominance of the

shorter C₂₃ and C₂₅ n-alkanes (e.g. Baas et al., 2000; Vonk and Gustafsson, 2009), whereas longer chain n-alkanes (C₂₇-C₃₃) are synthesized by higher plants (e.g., Pancost et al., 2002; Nichols et al., 2006) . Here we express the abundance of *Sphagnum* relative to higher plants as the proportion of C₂₃ and C₂₅ relative to the C₂₇-C₃₃ odd-carbon-numbered n-alkanes. Finally, the input of soil organic matter into the marine environment was estimated using the relative abundance of branched glycerol dialkyl glycerol tetraethers (brGDGTs), produced by bacteria that are abundant in soils, versus that of the marine Thaumarchaeota-derived isoprenoid GDGT crenarchaeol (Sinninghe Damsté et al., 2002), which is quantified in the Branched and Isoprenoid Tetraether (BIT) index (Hopmans et al., 2004). The distribution of brGDGTs in soils is temperature dependent (Weijers et al., 2007; Peterse et al., 2012). Annual mean air temperatures (MAT) were reconstructed based on down-core distributional changes of brGDGT and a global soil calibration that uses both the 5- and 6-methyl isomers of the brGDGTs (MAT_{mr}; De Jonge et al., 2014a). Cyclisation of Branched Tetraethers (CBT) ratios, was shown earlier to correlate with the ambient MAT and soil pH (Weijers et al., 2007; Peterse et al., 2012). The much improved CBT' ratio (De Jonge et al., 2014a), which includes the pH dependent 6-methyl brGDGTs, is used here to reconstruct soil pH. The Total Organic Carbon (TOC) and total nitrogen measurements are used to determine the atomic C/N ratio that in coastal marine sediments can indicate the dominant source of organic matter, with marine C/N values at ~10 and terrestrial between 15 and 30 (Hedges et al., 1997).

4.5 Organic geochemical processing

Organic geochemical analyses were limited to the core and sidewall core samples. For TOC determination ~ 0.3 g of freeze dried and powdered sediment was weighed, and treated with 7.5 ml 1 M HCL to remove carbonates, followed by 4 h shaking, centrifugation and decanting. This procedure was repeated with 12 h shaking. Residues were washed twice with

332 demineralised water dried at 40-50°C for 96 h after which weight loss was determined. ~15 to
333 20 mg ground sample was measured in a Fisons NA1500 NCS elemental analyzer with a
334 normal Dumas combustion setup. Results were normalized to three external standards (BCR,
335 atropine and acetanilide) analyzed before and after the series, and after each ten
336 measurements. % TOC was determined by %C x decalcified weight/original weight.

337
338 For biomarker extraction ca. 10 g of sediment was freeze dried and mechanically powdered.
339 The sediments were extracted with a Dichloromethane (DCM):Methanol (MeOH) solvent
340 mixture (9:1, v/v, 3 times for 5 min each) using an Accelerated Solvent Extractor (ASE,
341 Dionex 200) at 100°C and ca. 1000 psi. The resulting Total Lipid Extract (TLE) was
342 evaporated to near dryness using a rotary evaporator under near vacuum. The TLE then was
343 transferred to a 4 ml vial and dried under a continuous N₂ flow. A 50% split of the TLE was
344 archived. For the working other half elemental sulfur was removed by adding activated (in
345 2M HCl) copper turnings to the TLE in DCM and stirring overnight. The TLE was
346 subsequently filtered over Na₂SO₄ to remove the CuS, after which 500 ng of a C₄₆ GDGT
347 internal standard was added (Huguet et al., 2006). The resulting TLE was separated over a
348 small column (Pasteur pipette) packed with activated Al₂O₃ (2 h at 150°C). The TLE was
349 separated into an apolar, a ketone and a polar fraction by eluting with n-hexane : DCM 9:1
350 (v/v), n-hexane : DCM 1:1 (v/v) and DCM : MeOH 1:1 (v/v) solvent mixtures, respectively.
351 The apolar fraction was analyzed by gas chromatography (GC) coupled to a flame ionization
352 detector (FID) and gas chromatography/mass spectroscopy (GC/MS) for quantification and
353 identification of specific biomarkers, respectively. For GC, samples were dissolved in 55 µl
354 hexane and analyzed using a Hewlett Packard G1513A autosampler interfaced to a Hewlett
355 Packard 6890 series Gas Chromatography system equipped with flame ionization detection,
356 using a CP-Sil-5 fused silica capillary column (25 m x 0.32 mm, film thickness 0.12 µm),

with a 0.53 mm pre-column. Temperature program: 70°C to 130°C (0 min) at 20°C/min, then to 320°C at 4°C/min (hold time 20 mins). The injection volume of the samples was 1 µl.

Analyses of the apolar fractions were performed on a ThermoFinnigan Trace GC ultra, interfaced to a ThermoFinnigan Trace DSQ MS using the same temperature program, column and injection volume as for GC analysis. Alkane ratios are calculated using peak surface areas of the respective alkanes from the GC/FID chromatograms.

Prior to analyses, the polar fractions, containing the GDGTs, were dissolved in *n*-hexane : propanol (99:1, v/v) and filtered over a 0.45 µm mesh PTFE filter (ø 4mm). Subsequently, analyses of the GDGTs was performed using ultra high performance liquid chromatography-mass spectrometry (UHPLC-MS) on an Agilent 1290 infinity series instrument coupled to a 6130 quadrupole MSD with settings as described in Hopmans et al. (2016). In short, separation of GDGTs was performed on two silica Waters Acquity UHPLC HEB Hilic (1.7µm, 2.1mm x 150mm) columns, preceded by a guard column of the same material. GDGTs were eluted isocratically using 82% A and 18% B for 25 mins, and then with a linear gradient to 70% A and 30% B for 25 mins, where A is *n*-hexane, and B = *n*-hexane:isopropanol. The flow rate was constant at 0.2 ml/min. The [M+H]⁺ ions of the GDGTs were detected in selected ion monitoring mode, and quantified relative to the peak area of the C₄₆ GDGT internal standard.

5 Results

5.1 Stable isotope data

The glacial-interglacial range in *Cassidulina teretis* δ¹⁸O (δ¹⁸O_b) is ~1‰ between MIS 98 and 97, and ~1.3‰ between MIS 95 and 94, but with considerably more variation in especially MIS 95 (Fig. 3). The δ¹³C_b data co-vary consistently with δ¹⁸O_b and have a glacial-interglacial

range of $\sim 1.1\text{‰}$, besides one strongly depleted value in MIS 94 (-3.5‰). The MIS 95 $\delta^{13}\text{C}_b$ values are less variable than the $\delta^{18}\text{O}_b$, pointing to an externally forced signal in the latter. The $\delta^{18}\text{O}_b$ confirms the relation between glacial stages and fine grained sediment as proposed by Kuhlman et al. (2006a,b). Although the data are somewhat scattered, the A15-3/4 phase relation to the sediment facies is in agreement with the high-resolution stable isotope benthic foraminifera record of the onshore Noordwijk borehole (Noorbergen et al., 2015). The glacial to interglacial ranges are very similar in magnitude with those reported by Sosdian and Rosenthal (2009) for the North Atlantic, but on average lighter by $\sim 0.5\text{‰}$ ($\delta^{18}\text{O}_b$) and $\sim 1.8\text{‰}$ ($\delta^{13}\text{C}_b$).

5.2 Palynology

Palynomorphs, including dinocysts, freshwater palynomorphs and pollen, are abundant, diverse, and well-preserved in these sediments. Striking is the dominance by conifer pollen. Angiosperm (tree) pollen are present and diverse, but low in abundance relative to conifers. During interglacials (MIS 103, 99, 97, 95, and 93) the pollen record generally shows increased and more diverse tree pollen (particularly *Picea* and *Tsuga*), and warm temperate *Osmunda* spores, whereas during glacials (MIS 102, (100), 98, 96, and 94) herb and heath pollen indicative of open landscapes are dominant (Fig S2). The % arboreal pollen (AP; excl. bisaccate pollen) summarizes these changes, showing maximum values of $>40\%$ restricted to just a part of the coarser grained interglacial intervals (Fig. 3). The percentage record of cold water dinocysts is quite scattered in some intervals but indicates generally colder conditions within glacial stages, and minima during %AP maxima (Fig. 3). After peak cold conditions and a TOC maximum (see below), but still well within the glacials, the % Protoperidinoid consistently increases. Some intervals (e.g., top of MIS 94) are marked by influxes of freshwater algae (*Pediastrum* and *Botryococcus*), indicating a strong riverine input, these data

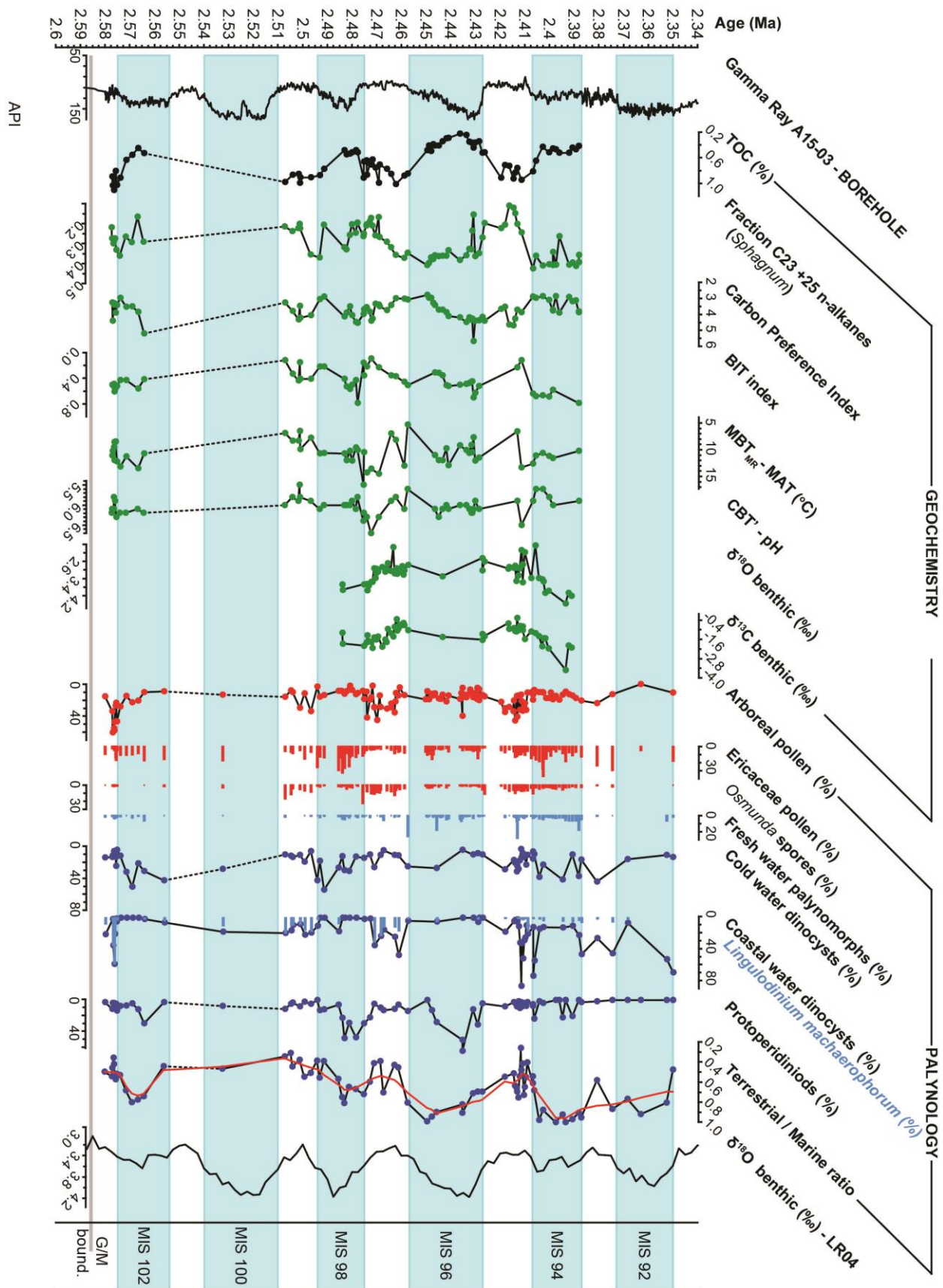
however do not indicate a clear trend. This robust in-phase pattern of glacial-interglacial variations is also reflected by high T/M ratios during glacials, indicating coastal proximity, and low T/M during (final phases of) interglacials. The Glacial-Interglacial (G-IG) variability in the T/M ratio is superimposed on a long-term increase. The coastal (warm-tolerant) dinocyst maxima are confined to the interglacial intervals and their abundance increases throughout the record. Successive increases of coastal inner neritic *Lingulodinium machaerophorum*, followed by increases in coastal lagoonal species in the youngest part, mirror the shoaling trend in the T/M ratio, which in time correspond with the gradual progradation of the Eridanos delta front (Fig. S1).

5.3 Organic geochemical proxies

The lowest TOC contents are reached in the clay intervals, and typically range between 0.5% in glacials and 1% in interglacials (Fig. 3). Nitrogen concentrations are relatively stable resulting in C/N ratios primarily determined by organic carbon content, ranging between ~8-9 (glacials) and ~14 and 17 (interglacials). The Carbon Preference Index (CPI) is generally high, reflecting a continuous input of immature terrestrial organic matter. Minimum CPI values of ~2.8 - 2.9 are reached at the transitions from the coarser sediments to the clay intervals after which they increase to maxima of 4.5 - 5.0 in the late interglacials. The *n*-C₂₃₊₂₅ *Sphagnum* biomarker correlates consistently with the T/M ratio, %AP, and cold water dinocysts (Fig. 3), while the variation in the CPI index is partially out of phase; it is more gradual and lags the % TOC and other signals. Generally lower Branched and Isoprenoid Tetraether (BIT) index values during interglacials (Fig. 3) indicate more marine conditions, i.e. larger distance to the coast and relatively reduced terrestrial input from the Eridanos catchment (cf. Sinninghe Damsté, 2016). As both brGDGT input (run off, soil exposure and erosion) and sea level (distance to the coast) vary across G-IG timescales, for example during

deglaciation and subsequent reactivation of fluvial transport (Bogaart and van Balen, 2000), the variability of the BIT index is somewhat different compared to the T/M palynomorph ratio (Fig. 3), but is generally in phase with gradual transitions along G-IG cycles. The MAT_{mr}-based temperature reconstructions vary between 5 and 17°C, reaching maximum values in MIS 97. However, in the MIS 99/98 and MIS 96/95 transitions the MAT_{mr} shows variability opposite to the identified G-IG cycles and the signal contains much high-order variability. Low values during interglacials generally coincide with low CBT'-reconstructed soil pH of <6.0 (Fig. 3).

Figure 3: spliced record of A15-3 and A15-4 showing the principal geochemical and palynological indices. Shaded blue intervals represent the identified glacial MIS delimited by the gamma-ray transitions following Kuhlmann et al. (2006a,b). Data density is dependent on type of sample as indicated in Fig. 1. Age scale is based on correlation and LOESS interpolation of the identified MIS transitions to the LR04 benthic stack (Lisiecki and Raymo, 2005) as shown in Fig S3. Data is available in Tables S2 and 3.



6 Discussion

6.1 Paleoenvironmental setting and climate signals

The source area study by Kuhlmann et al. (2004) indicated the Eridanos paleoriver as the principal source of the terrestrial deposits. The detailed seismic interpretations indeed show the advancing Eridanos delta front from the east toward the sites (Fig. S1). This trend is captured by the long-term increases in the T/M ratio and the proportion of coastal dinocysts (Fig. 3). In- or exclusion of bisaccate pollen in the T/M index (Fig. S5), the component most sensitive to differential transport processes, indicates no direct influence of differential transport on the T/M ratio. During MIS 103, 99, 97, 95, and 93 the AP% increases indicate generally warmer and more humid conditions than during MIS 102, 98, 96, and 94 (Fig. 3). The cold-water temperature signal based on dinocysts is more variable than the terrestrial cooling signals from the AP%. Pollen assemblages represent mean standing vegetation in the catchment, and also depend on dominant circulation patterns and short-term climate variations (Donders et al., 2009). Due to exclusion of bisaccate pollen, the %AP is generally low but eliminates any climate signal bias due to the direct effect of sea level changes (Donders et al., 2009; Kotthoff et al., 2014). In the record there are small but significant time lags between proxies, which have important implications for explaining the forcing of G-IG cycles. In the best constrained MIS transition (98 to 97), the G-IG transition is seen first in decreases of the cold water dinocysts and $n\text{-C}_{23+25}$ n-alkanes predominantly derived from *Sphagnum*. Subsequently the BIT decreases, and MAT_{mr} and the %AP increase, and finally the $\delta^{18}\text{O}_b$ and T/M ratio decrease with a lag of a few thousand years (Fig. 3). Changes in the CPI record are more gradual, but generally in line with T/M. The AP% and T/M proxies have the most extensive record and detailed analysis of several glacial-interglacial transitions shows that the declines in AP% consistently lead the T/M increases by 3-8 kyr based on the present age model (Fig. S2). The T/M ratio variability corresponds well to the LR04 benthic stack (Fig.

3), which is primarily an obliquity signal. Within the constraints of the sample availability, our record captures the approximate symmetry between glaciation and deglaciation typical of the Early Pleistocene (Lisiecki and Raymo, 2005).

The high variability and strongly depleted values in $\delta^{18}\text{O}_b$ during MIS 95 occur during peak coastal dinocyst abundances, suggesting high run off during maximum warming phases. During cold water dinocysts maxima, the high abundance of Protoperidinioids indicates high nutrient input, and productive spring/summer blooms, which point to strong seasonal temperature variations. This productivity signal markedly weakens in MIS 94 and 92 and the gradual T/M increase is consistent with the basin infill and gradually approaching shelf-edge delta (Fig. S1). As Protoperidinioid minima generally occur during TOC maxima there is no indication for a preservation overprint since selective degradation typically lowers relative abundances of these P-cysts (Gray et al., 2017). Combined, the high TOC and CPI values, coastal and stratified water conditions, and intervals of depleted $\delta^{18}\text{O}_b$ document increased Eridanos run-off during interglacials. These suggest a primarily terrestrial organic matter source that, based on mineral provenance studies (Kuhlmann et al., 2004) and high conifer pollen abundance documented here, likely originated from the Fennoscandian Shield. The fine-grained material during cold phases is probably transported by meltwater during summer from local glaciers that developed since the late Pliocene at the surrounding Scandinavian mainland (Mangerud et al., 1996; Kuhlmann et al., 2004).

6.2 Temperature reconstruction and brGDGT input

Whereas the BIT index reflects the G-IG cycles consistently, the MAT_{mr} record, which is based on GDGTs, has a variable phase relation with the G-IG cycles and high variability. The

500 use of MAT_{mr} in coastal marine sediments is based on the assumption that river-deposited
501 brGDGTs reflect an integrated signal of the catchment area. As the Eridanos system is
502 reactivated following glacials, glacial soils containing brGDGT are likely eroded causing a
503 mixed signal of glacial and interglacial material. The lowest MAT_{mr} and highest variability is
504 indeed observed during periods of deposition of sediments with a higher TOC content and
505 minima of CBT'-derived pH below 6 (Fig. 3), consistent with increased erosion of acidic
506 glacial (peat) soil. Additional analysis of the apolar fractions in part of the samples reveals
507 during these periods a relatively high abundance of the C₃₁ 17 α , 21 β -homohopanes, which in
508 immature soils indicates a significant input of acidic peat (Pancost et al., 2002). This suggests
509 that the variability in the MAT_{mr} record is not fully reliable due to (variable) erosion of glacial
510 soils or peats. Alternatively, the terrestrial brGDGT signal may be altered by a contribution of
511 brGDGTs produced in the marine realm. BrGDGTs were initially believed to be solely
512 produced in soils, but emerging evidence suggests that brGDGTs are also produced in the
513 river itself (e.g., Zell et al., 2013; De Jonge et al., 2014b) and in the coastal marine sediments
514 (e.g., Peterse et al., 2009; Sinninghe Damsté, 2016). Based on the modern system, the degree of
515 cyclisation of tetramethylated brGDGTs (#rings_{tetra}) has been proposed to identify a possible
516 in situ overprint (Sinninghe Damsté, 2016). The #rings_{tetra} in this sediment core is <0.37,
517 which is well below the suggested threshold of 0.7, and thus suggests that the brGDGTs are
518 primarily soil-derived. However, a ternary diagram of the brGDGT distribution show some
519 offset to the global soil calibration that decreases with increasing BIT values (Fig. S6),
520 pointing to some influence of in-situ GDGT production when terrestrial input is relatively
521 low. Finally, selective preservation in the catchment and during fluvial transport may have
522 affected the brGDGT signal, although experimental evidence on fluvial transport processes
523 indicates that these do not significantly affect initial soil-brGDGT compositions (Peterse et
524 al., 2015).

525

526 *6.3 Implications for the intensification of Northern Hemisphere glaciations*

527 The classic Milankovitch model predicts that global ice volume is forced by high northern
528 summer insolation (e.g. Hays et al., 1976). Raymo et al. (2006) suggested an opposite
529 response of ice sheets on both hemispheres due to precession forcing, cancelling out the
530 signal and amplifying obliquity in the early Pleistocene. That hypothesis predicts that regional
531 climate records on both hemispheres should contain a precession component that is not visible
532 in the sea level and deep sea $\delta^{18}\text{O}_b$ record, and is supported by evidence from Laurentide Ice
533 Sheet melt and iceberg-rafted debris of the East Antarctic ice sheet (Patterson et al., 2014;
534 Shakun et al., 2016). Alternatively, a dominantly obliquity forced G-IC cycle is supported by
535 a significant temperature component in the temperature deep sea $\delta^{18}\text{O}_b$ record (Sosdian and
536 Rosenthal, 2009) and dominant 41-kyr variability in North American biomarker dust fluxes.
537 Our results show that the regional NH climate on both land and sea surface vary on the same
538 timescale as the local relative sea level which, with the best possible age information so far
539 (Fig. S3), mirrors the global LR04 $\delta^{18}\text{O}_b$ record. The temperature changes lead the local sea
540 level by 3-8 kyr, which is consistent with a NH obliquity forcing scenario as cooling would
541 precede ice buildup and sea level change. Contrary to the model proposed by Raymo et al.
542 (2006), this suggests that the NH obliquity forcing is the primary driver for the glacial-
543 interglacial in the early Pleistocene, although we cannot exclude precession forcing as a
544 contributing factor.. Various studies indicate the importance of gradual CO_2 decline in the
545 intensification of NHG (Kürschner et al., 1996; Seki et al., 2010; Bartoli et al., 2011)
546 combined with the threshold effects of ice albedo (Lawrence et al., 2010; Etourneau et al.,
547 2010) and land cover changes (Koenig et al., 2011). Simulations of four coupled 3-D ice
548 models indicate that Antarctic ice volume increases respond primarily to sea-level lowering,
549 while Eurasian and North American ice sheet growth is initiated by temperature decrease (de

Boer et al., 2012). The latter dominate the eustatic sea-level variations during glacials. Our observations agree with the modelled temperature sensitivity of NH ice sheet growth. The dominant obliquity signal further suggests a seasonal aspect of the climate forcing. The combination of high summer productivity, based on increased *Protoperidinioid* dinocysts, and increased proportions of cold dinocysts during the glacials in the SNS record indicate a strong seasonal cycle. This confirms similar results from the North Atlantic (Hennissen et al., 2015) and is consistent with an obliquity-driven glacial-interglacial signal in a mid-latitudinal setting, likely promoting meridional humidity transport and ice buildup.

The southward migration of Arctic surface water masses indicated by increases in cold water dinocysts (Fig. 3) is furthermore relevant for understanding the relation between the Atlantic meridional overturning circulation (AMOC) intensity and ice sheet growth (e.g. Bartoli et al., 2005; Naafs et al., 2010). Mid-Pliocene increased heat transport and subsequent decrease during NHG due to AMOC intensity changes has been invoked from many proxy records but is difficult to sustain in models (Zhang et al., 2013). Our results indicate that the NW European early Pleistocene climate experienced significant cooling in all temperature-sensitive proxies during sea-level lowstands, which is consistent with southward displacement of the Arctic front and decreased AMOC (Naafs et al., 2010). The MAT_{mr} indicates a 4-6 °C glacial-interglacial amplitude although the timing is offset relative to the other proxies. The data-model mismatch in AMOC changes might be due to dynamic feedbacks in vegetation or (sea-) ice (Koenig et al., 2011; de Boer et al., 2012) that are prescribed variables in the model comparison by Zhang et al. (2013).

In addition, our SNS record provides a well-dated early Pleistocene Glacial-Interglacial succession integrating marine and terrestrial signals improving on the classic terrestrial Praetiglian stage. While conceptually valid, the earliest Pleistocene glacial stages defined in the continental succession of the SE Netherlands (Van der Vlerk and Florschütz, 1953; Zagwijn, 1960) and currently considered text book knowledge, are highly incomplete and locally varied (Donders et al., 2007). This shallow marine SNS record provides a much more suitable reflection of large-scale transitions and trends in NW Europe and merits further development by complete recovery of the sequence in a scientific drilling project (Westerhoff et al., 2016).

7 Conclusions

The independently dated late Pliocene-early Pleistocene sedimentary succession of the southern North Sea Basin provides a record that straddles the intensification of Northern Hemisphere Glaciation and the subsequent climate fluctuations in a shallow marine setting in great detail. The intensification of the glaciation and the correlation to marine isotope stages 103 to 92, including the conspicuous first Pleistocene glacial stages 98, 96 and 94, is well expressed in the marine and terrestrial palynomorph and organic biomarker records of the southern North Sea. The independent relative sea- and land-based temperature records show clearly coeval (at this resolution) expression of glacial-interglacial and sea-level cycles that are well-correlated to the LR04 benthic stack. Critically, both the biomarker signals, %AP, and cold water dinocyst variations show consistent in-phase variability on obliquity time scales, leading sea-level changes by 3-8 kyr, which supports a dominantly direct NH insolation control over early Pleistocene glaciations. Based on this integrated record, NH obliquity forcing is the primary driver for the glacial-interglacial cycles in the early

Pleistocene. Furthermore, our findings support the hypothesis of temperature sensitivity of NH ice sheet growth. The interglacials are characterized by (seasonally) stratified waters and/or near-shore conditions as glacial-interglacial cycles became more expressive and the Eridanos delta progressed into the region. The strong seasonality at mid-latitudes point to a vigorous hydrological cycling that should be considered as a potential factor in ice sheet formation in further investigations.

8 Author contributions

THD, HB and GK designed the research. NvH carried out the geochemical analyses under supervision of JW, GJR, FP and JSSD. RV, DM and THD carried out the palynological analyses and interpreted the data together with FS. LL and RPS provided stable isotope data on benthic foraminifera. JtV provided seismic interpretations. THD integrated the data and wrote the paper with contributions from all authors.

9 Acknowledgements

We are grateful the constructive comments of Stijn de Schepper and David Naafs and an anonymous referee that helped to improve the manuscript. We gratefully acknowledge the support in providing the offshore samples to this study and permission to publish by Wintershall Noordzee B.V., and project support by partners Chevron Exploration and Production Netherlands B.V., Total E&P Nederland B.V., Dana Petroleum Netherlands B.V., Oranje-Nassau Energie B.V., and Energie Beheer Nederland (EBN). Arnold van Dijk is thanked for running C/N and stable isotope analyses, and Giovanni Dammers for processing palynological samples. The work was partly supported by funding from the Netherlands Earth

System Science Center (NESSC) through a gravitation grant (NWO 024.002.001) from the Dutch Ministry for Education, Culture and Science to JSSD, GJR, and LL.

10 References

- Baas, M., Pancost, R., van Geel, B. Sinninghe Damsté, J.S., 2000. A comparative study of lipids in *Sphagnum* species. *Organic Geochemistry* 31: 535-539.
[https://doi.org/10.1016/S0146-6380\(00\)00037-1](https://doi.org/10.1016/S0146-6380(00)00037-1)
- Bakken, K. and Dale, B., 1986. Dinoflagellate cysts in Upper Quaternary sediments from southwestern Norway and potential correlations with the oceanic record. *Boreas* 15: 185-190. DOI: 10.1111/j.1502-3885.1986.tb00082.x
- Bartoli, G., Hönisch, B., Zeebe, R.E., 2011. Atmospheric CO₂ decline during the Pliocene intensification of Northern Hemisphere glaciations. *Paleoceanography* 26, PA4213.
<http://dx.doi.org/10.1029/2010PA002055>.
- Bijlsma, S., 1981. Fluvial sedimentation from the Fennoscandian area into the Northwest European Basin during the Late Cenozoic. *Geologie en Mijnbouw* 60: 337-345.
- Bogaart, P.W., van Balen, R.T., 2000. Numerical modeling of the response of alluvial rivers to Quaternary climate change. *Global and Planetary Change* 27: 147-163.
[https://doi.org/10.1016/S0921-8181\(01\)00064-9](https://doi.org/10.1016/S0921-8181(01)00064-9)
- Bray, E.E., and Evans, E.D., 1961. Distribution of n-paraffins as a clue to recognition of source beds. *Geochimica et Cosmochimica Acta* 22: 2-15. [https://doi.org/10.1016/0016-7037\(61\)90069-2](https://doi.org/10.1016/0016-7037(61)90069-2)
- Brierley, C.M., and Fedorov, A.V., 2010. Relative importance of meridional and zonal sea surface temperature gradients for the onset of the ice ages and Pliocene - Pleistocene climate evolution. *Paleoceanography* 25: PA2214. DOI:10.1029/2009PA001809.
- Brigham-Grette, J, Melles, M., Minyuk, P.S., Andreev, A.A., Tarasov, P.E., DeConto, R.M., König, S. Nowaczyk, N.R., Wennrich, V., Rosén, P., Haltia-Hovi, E., Cook, T.L., Gebhardt, C., Meyer-Jacob, C., Snyder, J.A., Herzschuh, U., 2013. Pliocene warmth, polar amplification, and stepped Pleistocene cooling recorded in NE Arctic Russia. *Science* 340: 1421-1427. DOI: 10.1126/science.1233137
- Caston, V.N.D., 1979. The Quaternary sediments of the North Sea. In: Banner, F.T., Collins, M.B., Massie, K.S. (Eds.), *The north-west European shelf seas: the sea bed and the sea in motion. I. Geology and Sedimentology*, Elsevier Oceanographic Series 24A, p. 195-270.

652 Dale, B., 1996. Dinoflagellate cyst ecology: modelling and geological applications. In: J.M.G.
653 Jansonius, D.C. (Editor), *Palynology: Principles and Application*, vol. 3. American
654 Association of Stratigraphic Palynologists Foundation, College Station, TX: 1249-1275.

655 de Boer, B., van de Wal, R.S.W., Lourens, L.J., Bintanja, R., Reerink, T.J., 2012. A
656 continuous simulation of global ice volume over the past 1 million years with 3-D ice-sheet
657 models. *Climate Dynamics* 41, 1365. doi:10.1007/s00382-012-1562-2

658 de Haas, H., Boer, W., van Weering, T.C.E., 1997. Recent sediment and organic carbon burial
659 in a shelf sea; the North Sea. *Marine Geology* 144, 131–146. [https://doi.org/10.1016/S0025-](https://doi.org/10.1016/S0025-3227(97)00082-0)
660 [3227\(97\)00082-0](https://doi.org/10.1016/S0025-3227(97)00082-0).

661 De Jonge, C., Hopmans, A.C., Zell, C.I., Kim, J.-H., Schouten, S., Sinninghe Damsté, J.S.,
662 2014a. Occurrence and abundance of 6-methyl branched glycerol dialkyl glycerol tetraethers
663 in soils: Implications for palaeoclimate reconstruction. *Geochimica et Cosmochimica Acta*
664 141: 97-112. <https://doi.org/10.1016/j.gca.2014.06.013>.

665 De Jonge, C., Stadnitskaia, A., Hopmans, E.C., Cherkashov, G., Fedotov, A. and Sinninghe
666 Damsté, J.S., 2014b. In-situ produced branched glycerol dialkyl glycerol tetraethers in
667 suspended particulate matter from the Yenisei River, Eastern Siberia. *Geochimica et*
668 *Cosmochimica Acta* 125: 476-491. <https://doi.org/10.1016/j.gca.2014.06.013>.

669 De Schepper, S., Head, M.J., and Louwye, S., 2009. Pliocene dinoflagellate cyst stratigraphy,
670 palaeoecology and sequence stratigraphy of the Tunnel-Canal Dock, Belgium, *Geological*
671 *Magazine* 146: 92-112. DOI: 10.1017/S0016756808005438.

672 De Schepper, S., Fischer, E.I., Groeneveld, J., Head, M.J., Matthiessen, J., 2011. Deciphering
673 the palaeoecology of Late Pliocene and Early Pleistocene dinoflagellate cysts.
674 *Palaeogeography, Palaeoclimatology, Palaeoecology* 309: 17–32.
675 <https://doi.org/10.1016/j.palaeo.2011.04.020>.

676 De Schepper, S., Groeneveld, J., Naafs, B.D.A., Van Renterghem, C., Hennissen, J., Head,
677 M.J., Louwye, S., Fabian, K., 2013. Northern Hemisphere glaciation during the globally
678 warm early Late Pliocene. *PLoS ONE* 8 (12), e81508.
679 <http://dx.doi.org/10.1371/journal.pone.0081508>.

680 de Vernal, A., 2009. Marine palynology and its use for studying nearshore environments,
681 *From Deep-Sea to Coastal Zones: Methods – Techniques for Studying Paleoenvironments*,
682 *IOP Conference Series: Earth and Environmental Science*, 5, 012002. DOI:10.1088/1755-
683 [1307/5/1/012002](https://doi.org/10.1088/1755-1307/5/1/012002).

684 Donders, T.H., Kloosterboer-van Hoeve, M.L., Westerhoff, W., Verreussel, R.H.C.M. &
685 Lotter, A.F., 2007. Late Neogene continental stages in NW Europe revisited. *Earth-Science*
686 *Reviews* 85: 161-186. <https://doi.org/10.1016/j.earscirev.2007.06.004>.

687 Donders, T.H., Weijers, J.W.H., Munsterman, D.K., Kloosterboer-van Hoeve, M.L., Buckles,
688 L.K., Pancost, R.D., Schouten, S., Sinninghe Damsté, J.S. & Brinkhuis, H., 2009. Strong

689 climate coupling of terrestrial and marine environments in the Miocene of northwest Europe.
690 Earth and Planetary Science Letters 281 (3-4): 215-225.
691 <https://doi.org/10.1016/j.epsl.2009.02.034>.

692 Eglinton, G., Hamilton, R.J., 1967. Leaf epicuticular waxes. Science 156, 1322-1335. DOI:
693 10.1126/science.156.3780.1322.

694 Etourneau, J., Schneider, R., Blanz, T., Martinez, P., 2010. Intensification of the Walker and
695 Hadley atmospheric circulations during the Pliocene-Pleistocene climate transition. Earth and
696 Planetary Science Letters 297: 103-110. <http://dx.doi.org/10.1016/j.epsl.2010.06.010>.

697 Faegri, K., Iversen, J., Kaland, P.E., Krzywinski, K., 1989. Text book of pollen analysis, IV
698 Edition. The Blackburn Press, 328 pp.

699 Gibbard P.L., and Lewin, J., 2016. Filling the North Sea Basin: Cenozoic sediment sources
700 and river styles. Geologica Belgica 19: 201-217. <http://dx.doi.org/10.20341/gb.2015.017>

701 Gray, D. D., Zonneveld, K.A., & Versteegh, G.J., 2017. Species-specific sensitivity of
702 dinoflagellate cysts to aerobic degradation: A five-year natural exposure experiment. Review
703 of Palaeobotany and Palynology 247, 175-187. DOI: 10.1016/j.revpalbo.2017.09.002

704 Head, M.J., 1996. Modern dinoflagellate cysts and their biological affinities. In: Jansonius, J.,
705 McGregor, D.C. (Eds.), Palynology: Principles and Application, vol. 3. American Association
706 of Stratigraphic Palynologists Foundation, College Station, TX, pp. 1197-1248.

707 Haug, G.H. and Tiedemann, R., 1998. Effect of the formation of the Isthmus of Panama on
708 Atlantic Ocean thermohaline circulation. Nature 393 (6686): 673- 676. DOI:10.1038/31447.

709 Haug, G.H., Sigman, D.M., Tiedemann, R., Pedersen, T.F. & Sarnthein, M., 1999. Onset of
710 permanent stratification in the subarctic Pacific Ocean. Nature 40: 779–782.
711 DOI:10.1038/44550

712 Haug, G.H., Ganopolski, A., Sigman, D.M., Rosell-Mele, A., Swann, G. E. A, Tiedemann, R.,
713 Jaccard, S. L., Bollmann, J., Maslin, M.A., Leng, M.J. and Eglinton, G., 2005. North Pacific
714 seasonality and the glaciation of North America 2.7 million years ago. Nature 433: 821-825.
715 DOI: 10.1038/nature03332.

716 Hays, J. D., Imbrie, J. & Shackleton, N. J., 1976. Variations in the Earth's orbit: pacemaker of
717 the ice ages. Science 194; 1121–1132. doi: 10.1126/science.194.4270.1121.

718 Head, M.J., Riding, J.B., Eidvin, T., Chadwick, R.A., 2004. Palynological and foraminiferal
719 biostratigraphy of (Upper Pliocene) Nordland Group mudstones at Sleipner, northern North
720 Sea. Marine and Petroleum Geology 21:277-297.
721 <http://dx.doi.org/10.1016/j.marpetgeo.2003.12.002>.

722 Hedges, J.I., Keil, R.G., & Benner, R., 1997. What happens to terrestrial organic matter in the
723 ocean? Organic Geochemistry 27: 195-212. [https://doi.org/10.1016/S0146-6380\(97\)00066-1](https://doi.org/10.1016/S0146-6380(97)00066-1)

724 Hennissen, J.A.I., Head, M.J., De Schepper, S., Groeneveld, J., 2015. Increased seasonality
 725 during the intensification of Northern Hemisphere glaciation at the Pliocene-Pleistocene
 726 transition ~2.6 Ma. *Quaternary Science Reviews* 129: 321–332.
 727 <https://doi.org/10.1016/j.quascirev.2015.10.010>.

728 Hennissen, J.A.I., Head, M.J., De Schepper, S., Groeneveld, J., 2017. Dinoflagellate cyst
 729 paleoecology during the Pliocene–Pleistocene climatic transition in the North Atlantic.
 730 *Palaeogeography, Palaeoclimatology, Palaeoecology* 470: 81–108.
 731 <https://doi.org/10.1016/j.palaeo.2016.12.023>.

732 Heusser, L.E., and Shackleton, N.J., 1979. Direct marine-continental correlation: 150,000-
 733 year oxygen isotope-pollen record from the North Pacific. *Science* 204: 837–839. DOI:
 734 10.1126/science.204.4395.837.

735 Hooghiemstra, H., 1988. Palynological records from Northwest African marine sediments: a
 736 general outline of the interpretation of the pollen signal. *Philosophical Transactions of the*
 737 *Royal Society of London, Series B Biological Sciences* 318 (1191): 431–449. DOI:
 738 10.1098/rstb.1988.0018.

739 Hooghiemstra, H., Ran, E.T.H., 1994. Late Pliocene-Pleistocene high resolution pollen
 740 sequence of Colombia: An overview of climatic change. *Quaternary International*, 21: 63–80

741 Hopmans, E.C., Weijers, J.W.H., Schefuss, E., Herfort, L., Sinninghe Damsté, J.S., Schouten,
 742 S., 2004. A novel proxy for terrestrial organic matter in sediments based on branched and
 743 isoprenoid tetraether lipids. *Earth and Planetary Science Letters* 24: 107–116.
 744 <https://doi.org/10.1016/j.epsl.2004.05.012>.

745 Hopmans, E.C., Schouten, S., Sinninghe Damsté, J.S., 2016. The effect of improved
 746 chromatography on GDGT-based palaeoproxies. *Organic Geochemistry* 93: 1–6.
 747 <https://doi.org/10.1016/j.orggeochem.2015.12.006>.

748 Huuse, M., Lykke-Andersen, H., Michelsen, O., 2001. Cenozoic evolution of the eastern
 749 North Sea Basin – new evidence from high-resolution and conventional seismic data. *Marine*
 750 *Geology* 177: 243–269.

751 Huybers, P., 2011. Combined obliquity and precession pacing of late Pleistocene
 752 deglaciations. *Nature* 480: 229–232. DOI:10.1038/nature10626.

753 Keigwin, L. D., 1982. Isotope paleoceanography of the Caribbean and east Pacific: role of
 754 Panama uplift in late Neogene time. *Science* 217: 350–353. DOI:
 755 10.1126/science.217.4557.350.

756 Kemna, H.A., Westerhoff, W.E., 2007. Remarks on the palynology-based chronostratigraphic
 757 subdivision of the Pliocene terrestrial deposits in NW-Europe. *Quaternary International* 164–
 758 165: 184–196. <https://doi.org/10.1016/j.quaint.2006.10.017>.

759 Kennicutt II, M.C., Barker, C., Brooks, J.M., DeFreitas, D.A., Zhu, G.H., 1987. Selected
760 organic matter source indicators in the Orinoco, Nile and Changjiang deltas. *Organic*
761 *Geochemistry* 11: 41-51. [https://doi.org/10.1016/0146-6380\(87\)90050-7](https://doi.org/10.1016/0146-6380(87)90050-7).

762 Knies, J., Cabedo-Sanz, P., Belt, S.T., Baranwal, S., Fietz, S., Rosell-Mele, A., 2014. The
763 emergence of modern sea ice cover in the Arctic Ocean. *Nature Communications* 5:
764 <http://dx.doi.org/10.1038/ncomms6608>.

765 Koenig, S.J., DeConto, R.M. & Pollard, D., 2011. Late Pliocene to Pleistocene sensitivity of
766 the Greenland Ice Sheet in response to external forcing and internal feedbacks. *Climate*
767 *Dynamics* 37: 1247. DOI:10.1007/s00382-011-1050-0.

768 Kotthoff, U., Greenwood, D., McCarthy, F., Müller-Navarra, K., Prader, S., Hesselbo, S.,
769 2014. Late Eocene to middle Miocene (33 to 13 million years ago) vegetation and climate
770 development on the North American Atlantic Coastal Plain (IODP Expedition 313, Site
771 M0027). *Climate of the Past* 10: 1523-1539. <https://doi.org/10.5194/cp-10-1523-2014>.

772 Kuhlmann, G. & Wong, T.E., 2008. Pliocene paleoenvironment evolution as interpreted
773 from 3D-seismic data in the southern North Sea, Dutch offshore sector. *Marine and Petroleum*
774 *Geology* 25: 173-189. <https://doi.org/10.1016/j.marpetgeo.2007.05.009>.

775 Kuhlmann, G., Pedersen, R.-B., de Boer, P., Wong, T.E., 2004. Provenance of Pliocene
776 sediments and paleoenvironmental change in the southern North Sea region using Sm/Nd
777 (samarium-neodymium) provenance ages and clay mineralogy. *Sedimentary Geology* 171:
778 205-226. DOI: 10.1016/j.sedgeo.2004.05.016.

779 Kuhlmann, G., Langereis, C.G., Munsterman, D., van Leeuwen, R.-J., Verreussel, R.,
780 Meulenkamp, J., Wong, T.E., 2006a. Chronostratigraphy of Late Neogene sediments in the
781 southern North Sea Basin and paleoenvironmental interpretations. *Palaeogeography,*
782 *Palaeoclimatology, Palaeoecology* 239: 426–455.
783 <https://doi.org/10.1016/j.palaeo.2006.02.004>.

784 Kuhlmann, G., Langereis, C.G., Munsterman, D., van Leeuwen, R.-J., Verreussel, R.,
785 Meulenkamp, J.E., Wong, Th.E., 2006b. Integrated chronostratigraphy of the Pliocene–
786 Pleistocene interval and its relation to the regional stratigraphical stages in the southern North
787 Sea region. *Netherlands Journal of Geosciences - Geologie en Mijnbouw* 85 (1): 19–35.
788 <https://doi.org/10.1017/S0016774600021405>.

789 Kürschner, W.A., van der Burgh, J., Visscher, H., and Dilcher, D.L., 1996. Oak leaves as
790 biosensors of late Neogene and early Pleistocene paleoatmospheric CO₂ concentrations.
791 *Marine Micropaleontology* 27: 299-312. [https://doi.org/10.1016/0377-8398\(95\)00067-4](https://doi.org/10.1016/0377-8398(95)00067-4).

792 Larsson, L.M., Dybkjaer, K., Rasmussen, E.S., Piasecki, S., Utescher, T., and Vajda, V.,
793 2011. Miocene climate evolution of northern Europe: A palynological investigation from
794 Denmark. *Palaeogeography, Palaeoclimatology, Palaeoecology* 309: 161-175.
795 <https://doi.org/10.1016/j.palaeo.2011.05.003>.

796 Lawrence, K.T., Sosdian, S., White, H.E., Rosenthal, Y., 2010. North Atlantic climate
 797 evolution through the Plio-Pleistocene climate transitions. *Earth and Planetary Science Letters*
 798 300: 329-342. <http://dx.doi.org/10.1016/j.epsl.2010.10.013>.

799 Lisiecki, L.E., and Raymo, M.E., 2005. A Pliocene-Pleistocene stack of 57 globally
 800 distributed benthic $\delta^{18}\text{O}$ records. *Paleoceanography* 20: PA1003.
 801 DOI:10.1029/2004PA001071.

802 Lister, A.M., 2004. The impact of Quaternary Ice Ages on mammalian evolution.
 803 *Philosophical Transactions of the Royal Society of London, Series B Biological Sciences* 359,
 804 221-241. DOI: doi: 10.1098/rstb.2003.1436.

805 Mackensen, A. & Hald, M., 1988. *Cassidulina teretis* Tappan and *C. laevigata* d'Orbigny:
 806 their modern and late Quaternary distribution in northern seas. *Journal of Foraminiferal*
 807 *Research* 18 (1): 16-24. DOI: <https://doi.org/10.2113/gsjfr.18.1.16>.

808 Mangerud, J., Jansen, E., Landvik, J., 1996. Late Cenozoic history of the Scandinavian and
 809 Barents Sea ice sheets. *Global and Planetary Change* 12: 11-26. [https://doi.org/10.1016/0921-](https://doi.org/10.1016/0921-8181(95)00009-7)
 810 [8181\(95\)00009-7](https://doi.org/10.1016/0921-8181(95)00009-7).

811 Maslin, M.A., Li, X. S., Loutre M. F., & Berger A. 1998. The contribution of orbital forcing
 812 to the progressive intensification of Northern Hemisphere Glaciation. *Quaternary Science*
 813 *Reviews* 17: 411-426. [https://doi.org/10.1016/S0277-3791\(97\)00047-4](https://doi.org/10.1016/S0277-3791(97)00047-4).

814 McCarthy, F.M.G. and Mudie, P., 1998. Oceanic pollen transport and pollen:dinocyst ratios
 815 as markers of late Cenozoic sea level change and sediment transport. *Palaeogeography,*
 816 *Palaeoclimatology, Palaeoecology* 138: 187-206. [https://doi.org/10.1016/S0031-](https://doi.org/10.1016/S0031-0182(97)00135-1)
 817 [0182\(97\)00135-1](https://doi.org/10.1016/S0031-0182(97)00135-1).

818 Meijer, T., Cleveringa, P., Munsterman, D.K., and Verreussel, R.M.C.H., 2006. The Early
 819 Pleistocene Praetigian and Ludhamian pollen stages in the North Sea Basin and their
 820 relationship to the marine isotope record. *Journal of Quaternary Science* 21: 307–310. DOI:
 821 10.1002/jqs.956.

822 Meloro, C., Raia, P., Carotenuto, F., Barbera, C., 2008. Diversity and turnover of Plio-
 823 Pleistocene large mammal fauna from the Italian Peninsula. *Palaeogeography,*
 824 *Palaeoclimatology, Palaeoecology* 268: 58-64. <https://doi.org/10.1016/j.palaeo.2008.08.002>.

825 Michelsen, O., Thomsen, E., Danielsen, M., Heilmann-Clausen, C., Jordt, H., Laursen, G-V.,
 826 1998. Cenozoic sequence stratigraphy in eastern North Sea. In: P.-C. de Graciansky, T.
 827 Jacquin, P.R. Vail and M.B. Farley (Eds), *Mesozoic and Cenozoic sequence stratigraphy of*
 828 *European Basins: SEPM (Society for Sedimentary Geology) Special Publications* 60, 91-118.
 829 DOI: <https://doi.org/10.2110/pec.98.02.0091>.

830 Mudelsee, M. and Raymo, M.E., 2005. Slow dynamics of the Northern Hemisphere
 831 glaciation. *Paleoceanography* 20, PA4022. DOI: 10.1029/2005PA001153.

832 Mudie, P.J. and McCarthy, F.M.G., 1984. Late Quaternary pollen transport processes, western
833 North Atlantic: Data from box models, cross-margin and N-S transects. *Marine Geology*, 118:
834 79-105. [https://doi.org/10.1016/0025-3227\(94\)90114-7](https://doi.org/10.1016/0025-3227(94)90114-7).

835 Naafs, B.D.A., Stein, R., Hefter, J., Khelifi, N., De Schepper, S., Haug, G.H., 2010. Late
836 Pliocene changes in the North Atlantic current. *Earth and Planetary Science Letters* 298: 434-
837 442. <http://dx.doi.org/10.1016/j.epsl.2010.08.023>.

838 Naafs, B.D.A., Hefter, J., Acton, G., Haug, G.H., Martínez-García, A., Pancost, R., Stein, R.,
839 2012. Strengthening of North American dust sources during the late Pliocene (2.7 Ma). *Earth*
840 *and Planetary Science Letters* 317-318. 8-19, doi:10.1016/j.epsl.2011.11.026

841 Naafs, B.D.A., Hefter, J., Stein, R., 2013. Millennial-scale ice rafting events and Hudson
842 Strait Heinrich(-like) Events during the late Pliocene and Pleistocene: a review. *Quaternary*
843 *Science Reviews* 80: 1-28. doi: 10.1016/j.quascirev.2013.08.014.

844 Nichols, J.E., Booth, R.K., Jackson, S.T., Pendall, E.G. & Huang, Y., 2006. Paleohydrologic
845 reconstruction based on n-alkane distributions in ombrotrophic peat. *Organic Geochemistry*
846 37: 1505-13. <https://doi.org/10.1016/j.orggeochem.2006.06.020>.

847 Noorbergen, L.J., Lourens, L.J., Munsterman, D. K., Verreussel, R.M.C.H., 2015. Stable
848 isotope stratigraphy of the early Quaternary of borehole Noordwijk, southern North Sea
849 .*Quaternary International* 386: 148 – 157. DOI:10.1016/j.quaint.2015.02.045.

850 Overeem, I., Weltje, G. J., Bishop-Kay, C., and Kroonenberg, S. B., 2001. The Late Cenozoic
851 Eridanos delta system in the Southern North Sea Basin: a climate signal in sediment supply?
852 *Basin Research* 13: 293-312. DOI: 10.1046/j.1365-2117.2001.00151.x.

853 Pagani, M., Liu, Z., LaRiviere, J., Ravelo, A.C., 2010. High Earth-system climate sensitivity
854 determined from Pliocene carbon dioxide concentrations. *Nature Geoscience*. 3: 27-30.
855 <http://dx.doi.org/10.1038/NGEO724>.

856 Pancost, R.D., Baas, M., van Geel, B., and Sinninghe Damsté, J.S., 2002. Biomarkers as
857 proxies for plant inputs to peats: an example from a sub-boreal ombrotrophic bog. *Organic*
858 *Geochemistry* 33(7): 675-690.

859 Pancost, R.D., Baas, M., van Geel, B., and Sinninghe Damsté, J.S., 2003. Response of an
860 ombrotrophic bog to a regional climate event revealed by macrofossil, molecular and carbon
861 isotopic data. *The Holocene*, 13(6): 921-932. [https://doi.org/10.1016/S0146-6380\(02\)00048-7](https://doi.org/10.1016/S0146-6380(02)00048-7).

862 Patterson, M.O., McKay, R., Naish, T., Escutia, C., Jimenez-Espejo, F.J., Raymo,
863 M.E., Meyers, S.R., Tauxe, L., Brinkhuis, H. & IODP Expedition 318 Scientists 2014. Orbital
864 forcing of the East Antarctic ice sheet during the Pliocene and Early Pleistocene. *Nature*
865 *Geoscience* 7: 841. DOI: 10.1038/ngeo2273.

866 Peterse, F., Moy, C.M., and Eglinton, T.I., 2015. A laboratory experiment on the behaviour of
867 soil-derived core and intact polar GDGTs in aquatic environments. *Biogeosciences* 12: 933–
868 943. DOI:10.5194/bg-12-933-2015.

869 Peterse, F., Kim, J.-H., Schouten, S., Kristensen, D.K., Koç, N. & Sinninghe Damsté, J.S.
870 2009. Constraints on the application of the MBT/CBT palaeothermometer at high latitude
871 environments (Svalbard, Norway). *Organic Geochemistry* 40 (6): 692-699.
872 <https://doi.org/10.1016/j.orggeochem.2009.03.004>.

873 Poore, H.R., Samworth, R., White, N.J., Jones, S.M., McCave, I.N., 2006. Neogene overflow
874 of Northern Component Water at the Greenland–Scotland Ridge. *Geochemistry Geophysics*
875 *Geosystems* 7. <http://dx.doi.org/10.1029/2005gc001085.Q06010>.

876 Pross, J. and Brinkhuis, H., 2005. Organic-walled dinoflagellate cysts as paleoenvironmental
877 indicators in the Paleogene; a synopsis of concepts. *Paläontologische Zeitschrift*, 79(1): 53-
878 59.

879 Quaijtaal, W., Donders, T.H., Persico, D. & Louwye, S., 2014. Characterising the middle
880 Miocene Mi-events in the Eastern North Atlantic realm - A first high-resolution marine
881 palynological record from the Porcupine Basin. *Palaeogeography, Palaeoclimatology,*
882 *Palaeoecology* 399: 140-159. <https://doi.org/10.1016/j.palaeo.2014.02.017>.

883 Ravelo, A.C., Andreasen, D.H., Lyle, M., Lyle, A.O., Wara, M.W., 2004. Regional climate
884 shifts caused by gradual global cooling in the Pliocene epoch. *Nature* 429 (6989): 263-267.
885 DOI:10.1038/nature02567

886 Ravelo, A.C., 2010. Palaeoclimate: Warmth and glaciation. *Nature Geoscience* 3: 672–674.
887 DOI:10.1038/ngeo965

888 Raymo, M.E., 1994. The initiation of Northern Hemisphere glaciation. *Annual Review of*
889 *Earth and Planetary Sciences* 22, 353-383.
890 <http://dx.doi.org/10.1146/annurev.earth.22.050194.002033>.

891 Raymo, M.E., Ruddiman, W.F., Backman, J., Clement, B. M., and Martinson, D.G., 1989.
892 Late Pliocene variation in Northern Hemisphere ice sheets and North Atlantic Deep Water
893 circulation. *Paleoceanography* 4: 413–446. DOI: 10.1029/PA004i004p00413.

894 Raymo, M. E., Lisiecki, L. & Nisancioglu, K.. 2006. Plio–Pleistocene ice volume, Antarctic
895 climate, and the global $\delta^{18}\text{O}$ record. *Science* 313: 492–495. DOI: 10.1126/science.1123296.

896 Reichert, G.J., Brinkhuis, H., 2003. Late Quaternary *Protoperidinium* cysts as indicators of
897 paleoproductivity in the northern Arabian Sea. *Marine Micropaleontology* 49 : 303-315.
898 [https://doi.org/10.1016/S0377-8398\(03\)00050-1](https://doi.org/10.1016/S0377-8398(03)00050-1).

899 Rieley, G., Collier, R.J., Jones, D.M., Eglinton, G., 1991. The biogeochemistry of Ellesmere
900 Lake, U.K. I: source correlation of leaf wax inputs to the sedimentary lipid record. *Organic*
901 *Geochemistry* 17: 901–912. [https://doi.org/10.1016/0146-6380\(91\)90031-E](https://doi.org/10.1016/0146-6380(91)90031-E).

902 Rochon, A., de Vernal, A., Turon, J.L., Mathiessen, J., Head, M.J., 1999. Distribution of
903 recent dinoflagellate cysts in surface sediments from the North Atlantic Ocean and adjacent
904 seas in relation to sea-surface parameters: American Association of Stratigraphic
905 Palynologists Foundation Contributions Series 35, 150 pp.

906 Rosoff, D.B., and Corliss, B.H., 1992. An analysis of Recent deep-sea benthic foraminiferal
 907 morphotypes from the Norwegian and Greenland seas. *Palaeogeography, Palaeoclimatology,*
 908 *Palaeoecology* 91, 13-20. [https://doi.org/10.1016/0031-0182\(92\)90028-4](https://doi.org/10.1016/0031-0182(92)90028-4).

909 Ruddiman, W.F., Raymo, M., McIntyre, A., 1986. Matuyama 41,000-year cycles: North
 910 Atlantic Ocean and northern hemisphere ice sheets: *Earth and Planetary Science Letters* 80:
 911 117-129. [https://doi.org/10.1016/0012-821X\(86\)90024-5](https://doi.org/10.1016/0012-821X(86)90024-5).

912 Sangiorgi, F. and Donders, T.H., 2004. Reconstructing 150 years of eutrophication in the
 913 north-western Adriatic Sea (Italy) using dinoflagellate cysts, pollen and spores. *Estuarine,*
 914 *Coastal and Shelf Science* 60: 69-79. <https://doi.org/10.1016/j.ecss.2003.12.001>.

915 Sangiorgi, F., Fabbri, D., Comandini, M., Gabbianelli, G. & Tagliavini, E., 2005. The
 916 distribution of sterols and organic-walled dinoflagellate cysts in surface sediments of the
 917 North-western Adriatic Sea (Italy). *Estuarine, Coastal and Shelf Science* 64: 395-406.

918 Shakun, J.D., Raymo, M.E., Lea, D.W., 2016. An early Pleistocene Mg/Ca- $\delta^{18}\text{O}$ record from
 919 the Gulf of Mexico: Evaluating ice sheet size and pacing in the 41-kyr world.
 920 *Paleoceanography* 31: 1011-1027. DOI: 10.1002/2016PA002956.

921 Seki, O., Foster, G.L., Schmidt, D.N., Mackensen, A., Kawamura, K., Pancost, R.D., 2010.
 922 Alkenone and boron-based Pliocene pCO₂ records. *Earth and Planetary Science Letters* 292:
 923 201-211. <http://dx.doi.org/10.1016/j.epsl.2010.01.037>.

924 Shackleton, N.J. and Hall, M.A., 1984. Oxygen and carbon isotope stratigraphy of Deep Sea
 925 Drilling Project Hole 552A: Plio- Pleistocene glacial history. D-G. Roberts. D. Schnitker et al.
 926 initial Reports of the Deep Sea Drilling Project 81: 599-609. U.S. Govt. Printing Office,
 927 Washington.

928 Schreck, M., Meheust, M., Stein, R. and Matthiessen, J., 2013. Response of marine
 929 palynomorphs to Neogene climate cooling in the Iceland Sea (ODP Hole 907A). *Marine*
 930 *Micropaleontology* 101: 49-67. <https://doi.org/10.1016/j.marmicro.2013.03.003>.

931 Sinninghe Damsté, J.S., Schouten, S., Hopmans, E.C., van Duin, A.C.T., Geenevasen, J.A.J.,
 932 2002. Crenarchaeol: the characteristic core glycerol dibiphytanyl glycerol tetraether
 933 membrane lipid of cosmopolitan pelagic crenarchaeota. *Journal of Lipid Research* 43: 1641-
 934 1651. doi: 10.1194/jlr.M200148-JLR200

935 Sinninghe Damsté, J.S., 2016. Spatial heterogeneity of sources of branched tetraethers in shelf
 936 systems - The geochemistry of tetraethers in the Berau River delta (Kalimantan, Indonesia).
 937 *Geochimica et Cosmochimica Acta* 186: 13-31. <https://doi.org/10.1016/j.gca.2016.04.033>.

938 Sluijs, A., Pross, J., and Brinkhuis, H., 2005. From greenhouse to icehouse; organic-walled
 939 dinoflagellate cysts as paleoenvironmental indicators in the Paleogene. *Earth Science*
 940 *Reviews* 68: 281-315. <https://doi.org/10.1016/j.earscirev.2004.06.001>.

941 Sørensen, J. C., Gregersen, U., Breiner, M. and O. Michelsen, 1997. High-frequency sequence
 942 stratigraphy of Upper Cenozoic deposits in the central and southeastern North Sea areas.

943 Marine and Petroleum Geology 14 (2): 99-123. <https://doi.org/10.1016/S0264->
944 8172(96)00052-9

945 Sosdian, S. Rosenthal, Y., 2009. Deep-sea temperature and ice volume changes across the
946 Pliocene-Pleistocene climate transitions. *Science* 325: 306-310.
947 DOI:10.1126/science.1169938 pmid:19608915.

948 Tabor, C.R., Poulsen, C.J., Pollard, D., 2014. Mending Milankovitch's theory: obliquity
949 amplification by surface feedbacks. *Climate of the Past* 10: 41–50. DOI: 10.5194/cp-10-41-
950 2014.

951 Thöle, H., Gaedicke, C., Kuhlmann, G., and Reinhardt, L., 2014. Late Cenozoic sedimentary
952 evolution of the German North Sea – A seismic stratigraphic approach. *Newsletters on*
953 *Stratigraphy* 47: 299–329. DOI: 10.1127/0078-0421/2014/0049.

954 Tzedakis, P.C., Crucifix, M., Mitsui, T., Wolff, E.W., 2017. A simple rule to determine which
955 insolation cycles lead to interglacials. *Nature* 542: 427–432 DOI:10.1038/nature21364.

956 Svenning, J.-C., 2003. Deterministic Plio-Pleistocene extinctions in the European cool-
957 temperate tree flora. *Ecology Letters* 6: 646–653. DOI: 10.1046/j.1461-0248.2003.00477.x.

958 Westerhoff, W., Donders, T.H. & Luthi, S.M., 2016. Report on ICDP workshop CONOSC
959 (COring the North Sea Cenozoic). *Scientific Drilling* 21: 47-51. <https://doi.org/10.5194/sd->
960 21-47-2016.

961 Whitehead, D.R., (1983). Wind pollination: some ecological and evolutionary perspectives.
962 In: Real, L. (Ed.), *Pollination Biology*. Academic Press, Orlando, pp.

963 Williams, G.L., Fensome, R.A., and MacRae, R.A., 2017. The Lentin and Williams index of
964 fossil dinoflagellates 2004 edition. American Association of Stratigraphic Palynologists,
965 Contributions Series 48, College Station, TX, 1097 pp. 97–108

966 Van der Vlerk, I.M, Florschütz, F. 1953. The palaeontological base of the subdivision of the
967 Pleistocene in the Netherlands. *Verhandelingen Koninklijke Nederlandse Akademie van*
968 *Wetenschappen, Afdeling Natuurkunde*, 1e Reeks XX(2): 1–58.

969 Versteegh, G.J.M., Zonneveld, K.A.F., 1994. Determination of (palaeo-)ecological
970 preferences of dinoflagellates by applying detrended and canonical correspondence analysis
971 to late Pliocene dinoflagellate cyst assemblages of the south Italian Singa section. *Review of*
972 *Palaeobotany and Palynology* 84: 181–199. [https://doi.org/10.1016/0034-6667\(94\)90050-7](https://doi.org/10.1016/0034-6667(94)90050-7).

973 Vonk, J.E., Gustafsson, Ö, 2009. Calibrating n-alkane *Sphagnum* proxies in sub-Arctic
974 Scandinavia. *Organic Geochemistry* 40: 1085-1090.
975 <https://doi.org/10.1016/j.orggeochem.2009.07.002>.

976 Zagwijn, W.H., 1960. Aspects of the Pliocene and early Pleistocene vegetation in The
977 Netherlands. *Mededelingen van de Geologische Stichting, Serie C* III-1–5, 1–78.

978 Zell, C., Kim, J.-H., Moreira-Turcq, P., Abril, G., Hopmans, E.C., Bonnet, M.-P., Sobrinho,
 979 R. L., and Sinninghe Damsté, J.S., 2013. Disentangling the origins of branched tetraether
 980 lipids and crenarchaeol in the lower Amazon River: implications for GDGT-based proxies,
 981 *Limnology and Oceanography*. 58, 343–353. DOI: 10.4319/lo.2013.58.1.0343.

982 Zhang, Z.-S., Nisancioglu, K. H., Chandler, M. A., Haywood, A. M., Otto-Bliesner, B. L.,
 983 Ramstein, G., Stepanek, C., Abe-Ouchi, A., Chan, W.-L., Bragg, F. J., Contoux, C., Dolan, A.
 984 M., Hill, D. J., Jost, A., Kamae, Y., Lohmann, G., Lunt, D. J., Rosenbloom, N. A., Sohl, L. E.,
 985 and Ueda, H., 2013. Mid-pliocene Atlantic Meridional Overturning Circulation not unlike
 986 modern. *Climate of the Past* 9, 1495-1504. DOI :10.5194/cp-9-1495-2013

987 Ziegler, P.A., 1990. Geological Atlas of Western and Central Europe (2nd edition). Shell
 988 Internationale Petroleum Maatschappij B.V.; Geological Society Publishing House (Bath),
 989 239 pp.

990 Zöllmer, V. and Irion, G., 1996. Tonminerale des Nordseeraumes ihr Verteilungsmuster in
 991 kreidezeitlichen bis pleistozänen Sedimentabfolgen und in den Oberflächensedimenten der
 992 heutigen Nordsee: Courier Forschungsinstitut Senckenberg, 190. Frankfurt am Mainz, 72 p.

993 Zonneveld, K.A.F., Marret, F., Versteegh, G.J.M., Bogus, K., Bonnet, S., Bouimetarhan, I.,
 994 Crouch, E., de Vernal, A., Elshanawany, R., Edwards, L., Esper, O., Forke, S., Grøsfjeld, K.,
 995 Henry, M., Holzwarth, U., Kieft, J.-F., Kim, S.-Y., Ladouceur, S., Ledu, D., Chen, L.,
 996 Limoges, A., Londeix, L., Lu, S.-H., Mahmoud, M.S., Marino, G., Matsouka, K.,
 997 Matthiessen, J., Mildenhall, D.C., Mudie, P., Neil, H.L., Pospelova, V., Qi, Y., Radi, T.,
 998 Richerol, T., Rochon, A., Sangiorgi, F., Solignac, S., Turon, J.-L., Verleye, T., Wang, Y. &
 999 Young, M., 2013. Atlas of modern dinoflagellate cyst distribution based on 2405 data points.
 1000 *Review of Palaeobotany and Palynology* 191: 1-197.
 1001 <https://doi.org/10.1016/j.revpalbo.2012.08.003>.

1002